CrossMark

Detection of Diatomic Carbon in 2I/Borisov

Hsing Wen Lin (林省文)[1] ●, Chien-Hsiu Lee (李見修)[2] ●, D. W. Gerdes[1,3] ●, Fred C. Adams[1,3] ●, Juliette Becker[4] ●,
Kevin Napier[1] ●, and Larissa Markwardt[3]

[1] Department of Physics, University of Michigan, Ann Arbor, MI 48109, USA; hsingwel@umich.edu
[2] NSF National Optical Infrared Astrophysical Research Laboratory, Tucson, AZ 85719, USA
[3] Department of Astronomy, University of Michigan, Ann Arbor, MI 48109, USA
[4] Division of Geological and Planetary Sciences, California Institute of Technology, Pasadena, CA 91125, USA
Received 2019 December 11; revised 2020 January 9; accepted 2020 January 14; published 2020 January 27

Abstract

2I/Borisov is the first-ever observed interstellar comet (and the second detected interstellar object (ISO)). It was discovered on 2019 August 30 and has a heliocentric orbital eccentricity of ~3.35, corresponding to a hyperbolic orbit that is unbound to the Sun. Given that it is an ISO, it is of interest to compare its properties—such as composition and activity—with the comets in our solar system. This study reports low-resolution optical spectra of 2I/Borisov. The spectra were obtained by the MDM Observatory Hiltner 2.4 m telescope/Ohio State Multi-Object Spectrograph (on 2019 October 31.5 and November 4.5, UT). The wavelength coverage spanned from 3700 to 9200 Å. The dust continuum reflectance spectra of 2I/Borisov show that the spectral slope is steeper in the blue end of the spectrum (compared to the red). The spectra of 2I/Borisov clearly show CN emission at 3880 Å, as well as C_2 emission at both 4750 and 5150 Å. Using a Haser model to covert the observed fluxes into estimates for the molecular production rates, we find $Q(CN) = 2.4 \pm 0.2 \times 10^{24}$ s^{-1}, and $Q(C_2) = (5.5 \pm 0.4) \times 10^{23}$ s^{-1} at the heliocentric distance of 2.145 au. Our $Q(CN)$ estimate is consistent with contemporaneous observations, and the $Q(C_2)$ estimate is generally below the upper limits of previous studies. We derived the ratio $Q(C_2)/Q(CN) = 0.2 \pm 0.1$, which indicates that 2I/Borisov is depleted in carbon-chain species, but is not empty. This feature is not rare for the comets in our solar system, especially in the class of Jupiter-family comets.

Unified Astronomy Thesaurus concepts: Comets (280)

Supporting material: data behind figure

1. Introduction

The detection of the first interstellar object (ISO), known as 'Oumuamua (Meech et al. 2017), has ushered in a new field of astronomy—the search and study of interloping minor bodies passing through the solar system. Within two years of the discovery of the first ISO, the second ISO, known as 2I/Borisov (Guzik et al. 2019), was discovered. 2I/Borisov is markedly different from 'Oumuamua. The new object is likely larger and displays a prominent cometary tail (Bolin et al. 2019; Jewitt & Luu 2019; Lee et al. 2019; Ye et al. 2019; Jewitt et al. 2020), and thus provides a unique opportunity to study the composition of comets originating from other planetary systems.

Upon the arrival of 2I/Borisov, it was studied observationally using follow-up imaging and spectroscopy. de León et al. (2019) obtained optical spectra with the 10 m GTC telescope and reported a spectral shape similar to that of D-type asteroids. Fitzsimmons et al. (2019) acquired optical spectra with the William Herschel Telescope (specifically at wavelengths shorter than the observations of de León et al. 2019) and presented the first detection of CN emission at 3880 Å. Kareta et al. (2019) carried out optical spectroscopic observations of the comet with MMT and the Large Binocular Telescope (LBT) at the heliocentric distance above 2.4 au but only obtained nondetection of diatomic carbon C_2. From the upper limit of $Q(CN)/Q(C_2)$ ratio, Kareta et al. (2019) concluded that 2I/Borisov is a carbon-depleted comet, similar to the Jupiter-family comets (JFCs) that are seen in our solar system. Opitom et al. (2019) investigated the C_2 emission from the Willian Herschel Telescope (WHT) observations when 2I/Borisov was

2.36 au away from the Sun, but also did not detect C_2. Nevertheless, both Kareta et al. (2019) and Opitom et al. (2019) concluded that 2I/Borisov is a carbon-depleted comet, and possibly exhausted its surface material before leaving its natal planetary system. As 2I/Borisov is still on an inbound trajectory toward the Sun, its cometary activity will increase, and we are likely to detect C_2 emission as the object approaches perihelion. In addition to CN and C_2, [O I] at 6300 Å was also detected and indicates that 2I/Borisov may also contain water ice (McKay et al. 2019). However, the absorption features of water ice in near-infrared have not been detected on the observations before early 2019 October (Yang et al. 2020).

This present work has three principal objectives. The first is to conduct continuous monitoring of 2I/Borisov, with the goal of revealing C_2 emission. The second is to use the observed $Q(CN)/Q(C2)$ ratio to constrain the surface properties of 2I/Borisov. The final objective is to investigate the evolution of both production rates $Q(CN)$ and $Q(C2)$ as a function of heliocentric distance, specifically as 2I/Borisov approaches perihelion.

2. Observation and Data Reduction

2I/Borisov was observed with the Hiltner 2.4 m telescope and the Ohio State Multi-Object Spectrograph (OSMOS; Martini et al. 2011) on 2019 October 31.5 and November 4.5 UT via the queue observations of MDM Observatory. The observational circumstances are listed in Table 1. The high throughput triplet prism mode of OSMOS was used to obtain low-resolution spectra. The triplet prism produces variable

Table 1
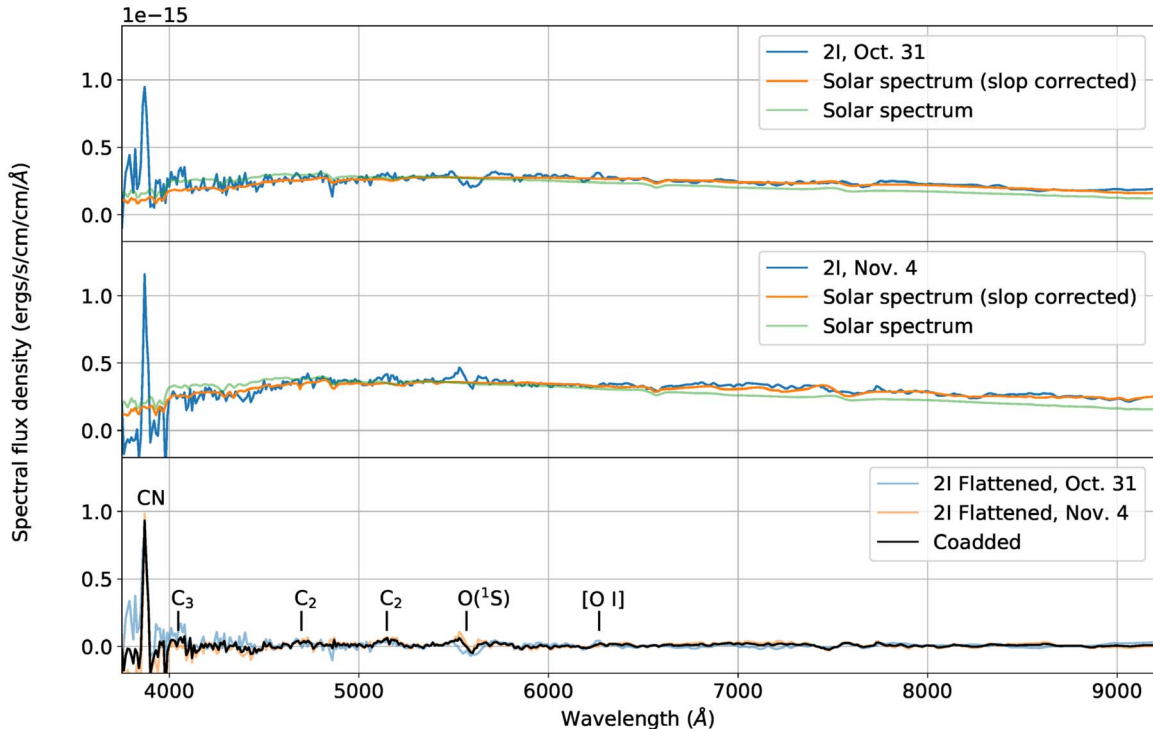### Log of Observations and Production Rates of 2I/Borisov

Date (UT)	r_h (au)[a]	Δ (au)[b]	Exp Time (s)	Airmass	$Q(CN)$ (s^{-1})	$Q(C_2)$ (s^{-1})[c]
2019 Oct 31.5	2.177	2.437	6×300	1.64–1.46	$(2.0 \pm 0.2) \times 10^{24}$	...
2019 Nov 4.5	2.145	2.373	11×300	1.91–1.47	$(2.4 \pm 0.2) \times 10^{24}$	$(5.5 \pm 0.4) \times 10^{23}$

Notes.
[a] Heliocentric distance.
[b] Geocentric distance.
[c] $Q(C_2)$ estimated from coadded all of the usable spectra.

Figure 1. 2I/Borisov spectra obtained by the Hiltner 2.4 m telescope/OSMOS. Top: 2019 October 31. Middle: 2019 November 4. The fitted solar analog spectra and slope-corrected (see Section 3.1) solar spectra are also shown. Bottom: flattened spectra with the solar spectrum removed. Note that the absorption/emission feature around 5600 Å is the O(^{1}S) band due to the non-proper sky subtraction, not the feature of the comet.

(The data used to create this figure are available.)

resolution of $\lambda/\Delta\lambda = 400$–60 across the wavelength range from 3600 to 10000 Å (Martini et al. 2011). The higher resolution of the triplet prism for the short wavelengths is ideal for the detection of gas emissions, i.e., CN and C$_2$, and the wide wavelength coverage is suitable to study the spectral type of the dust coma. The Hiltner 2.4 m telescope cannot guide non-sidereally. As a result, we observed with sidereal tracking and aligned the slit with the motion direction of 2I/Borisov (at PA = 143°). On 2019 October 31 UT we obtained 6 exposures and November 4 UT 11 exposures. Each exposure was 300 s and obtained with a 3″ wide slit.

Along with 2I/Borisov, we also observed G191-B2B (2019 October 31 UT) and BD28-4211 (2019 November 4 UT) as flux standards, planetary nebula IC351 as a wavelength calibrator, as well as G2 stars HIP 117367 (2019 October 31 UT) and HIP 117537 (2019 November 4 UT) as solar analogs.

Since the comet was moving across the slit, we were able to reconstruct the local sky background by combining the set of exposures. We subtracted bias and sky, and then extracted one-dimensional spectra with 27″.8 widths to maximize the signal

of the comet. The one-dimensional spectra had wavelength solutions derived via comparing the emission lines of planetary nebula IC351 (Feibelman et al. 1996) and also flux calibrated with a standard KPNO extinction correction applied. Although the OSMOS/triplet prism has a wavelength range from 3600 to 10000 Å, we were only able to identify the emission lines between 3835 (H9) and 9069 Å ([S III]). Therefore, we chopped the one-dimensional spectra, and only kept the wavelength between 3750 and 9200 Å to avoid too much extrapolation. The remaining 3750–9200 Å range should have a sufficiently accurate wavelength solution. The final reduction results of 2I/Borisov spectra are shown in Figure 1.

3. Analysis and Results

3.1. The Dust Continuum

The low-resolution spectra from 3750 to 9200 Å allow the measurement of the coma dust reflectance across the whole visible wavelength range. We divided the 2I/Borisov spectra (Figure 1, 2I) by solar analogs (Figure 1, solar spectrum) in
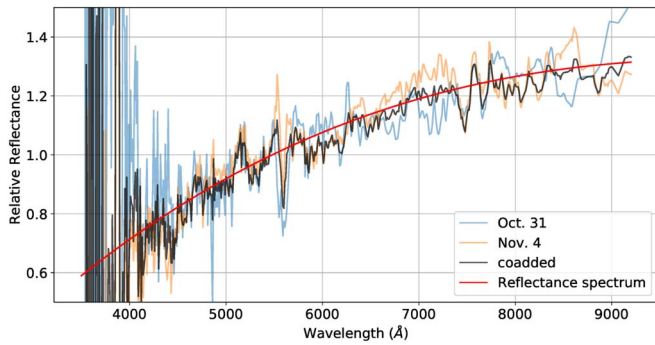
Figure 2. Reflectance spectrum of 2I/Borisov. A cubic spline is also plotted to model the trends of spectral slope variation.

Figure 3. Magnified spectra of 2I/Borisov from 3750 to 5400 Å.

order to normalize the reflectance spectrum, where the equality point is taken to be 5500 Å. We then coadded the spectra observed on 2019 October 31 and November 4 by weighting them by their total exposure time. The general slope of the reflectance spectrum varies with wavelength. As a result, we fitted the spectrum with a cubic spline to specify the spectral slope as a function of wavelength. The result is shown in Figure 2. The spectral slope is steeper in the shorter wavelength range than in the longer wavelength range. More specifically, we found an average slope of $19.3\%/10^3$ Å in the range of 3900 Å $< \lambda < 6000$ Å, and an average slope of $9.2\%/10^3$ Å in the range of 5500 Å $< \lambda < 9000$ Å. This result is consistent with both the blue-end slope reported by Fitzsimmons et al. (2019; $19.9 \pm 1.5\%/10^3$ Å) and Kareta et al. (2019; $22\%/10^3$ Å) and the red-end slope reported by de León et al. (2019; $10 \pm 1\%/10^3$ Å) and Kareta et al. (2019; $11\%/10^3$ Å). Such a result agrees with the spectral behavior of scattered light of micron-sized coma dust grains, which are commonly found within normal solar system comets (Jewitt & Meech 1986).

3.2. CN Emission and Production Rate

The 2I/Borisov spectra can be flattened by subtracting the solar spectrum, with the correction applied for the spectral slope, as described in Section 3.1. The flattened spectra are shown in the bottom panel of Figure 1. We identified gas emission lines in these processed spectra. The first feature is the clear CN(0–0) emission at 3880 Å. The flux of CN emission was directly measured by fitting a Gaussian function and giving a value of $(2.3 \pm 0.2) \times 10^{-14}$ ergs s^{-1} cm^{-2} on 2019 October 31 and $(2.9 \pm 0.2) \times 10^{-14}$ ergs s^{-1} cm^{-2} on 2019 November 4.

To convert the observed flux into a gas production rate, we first obtained fluorescence efficiency of CN from Schleicher (2010) to calculate the number of CN molecules within the extraction aperture. We then used a simple Haser model (Haser 1957) from `sbpy` (Mommert et al. 2019) to calculate the production rate of CN. The scale lengths of the parent (HCN, assuming CN gas is only generated by the photo-dissociation of this parent molecule) and daughter molecule (CN) were taken from A'Hearn et al. (1995), and we used the outflow velocity $0.85 \times r_h^{-0.5} = 0.58$ km s^{-1} (Cochran & Schleicher 1993). Because the Haser model is spherically symmetric, we integrate the Haser model with a $13\farcs9$ radius circular aperture and adjust the value to the equivalent area of our $3''$ by $27\farcs8$ aperture to derive the corresponding production rate of CN. We found $Q(\mathrm{CN}) = (2.0 \pm 0.2) \times 10^{24}$ s^{-1} on
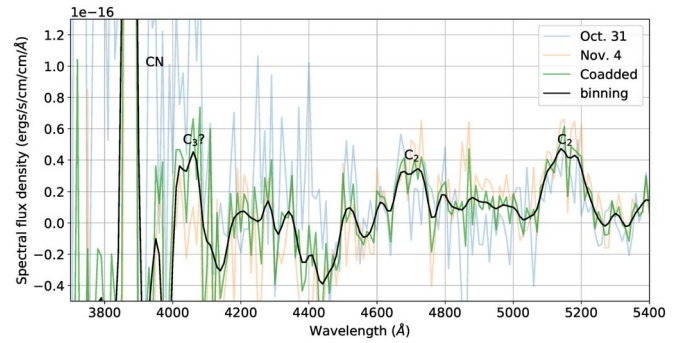
2019 October 31 and $(2.4 \pm 0.2) \times 10^{24}$ s^{-1} on 2019 November 4. This result is consistent with the previous $Q(\mathrm{CN})$ estimates from 2019 October (Kareta et al. 2019; Opitom et al. 2019) and suggests that the CN production rate of 2I/Borisov did not increase dramatically as it approached perihelion (over this time interval).

3.3. Possible C_3 Emission

In addition to the CN emission, we used the coadded spectrum to search for other weaker features across the entire wavelength range. We found the excess emission near the wavelengths corresponding to the C_3 and C_2 bands. The magnified (zoomed-in) spectrum in the wavelength range 3750 to 5400 Å is shown in Figure 3. The excess at 4050 Å matches the wavelength appropriate for C_3 emission. However, considering that this excess could be driven by the noisy data taken on 2019 October 31 (see Figure 3), we do not have sufficient confidence to claim the detection of C_3. However, if the possible C_3 emission is real, we estimate a flux $F = (2 \pm 1) \times 10^{-15}$ ergs s^{-1} cm^{-2} (extracted from the coadded but unbinned spectrum).

We calculated the C_3 production rate using the same method of Section 3.2 with a fluorescence efficiency of C_3 and the scale lengths of the parent/daughter molecule adopted from A'Hearn et al. (1995). Assuming that the outflow velocity is 0.58 km s^{-1} and that (again) this emission is real, we find $Q(C_3) = (3 \pm 1) \times 10^{22}$ s^{-1}. Note that this value is below the upper limit of $< 2 \times 10^{23}$ s^{-1} found in Opitom et al. (2019), and hence is consistent.

3.4. C_2 Emission and Production Rate

The other two excesses are located at 4700 and 5150 Å, which match the locations of $C_2(\Delta v = 1)$ and $C_2(\Delta v = 0)$ emissions, respectively. Unlike the excess near the C_3 band, however, the C_2 emission excesses were observed in both spectra; this consistency indicates that these features represent the detection of C_2 emission. The only potential issue is that the shapes of C_2 emission features are not exactly what is expected, in that we do not see sharp breaks in the longer wavelength sides. However, considering the effects of binning data, low spectral resolution, and low signal-to-noise ratio, it is highly possible to lose or smooth out the shapes of the C_2 emission features.

We measured the C_2 emission fluxes via the coadded but unbinned spectrum, and derived the $C_2(\Delta v = 0)$ flux $F = (5.7 \pm 0.4) \times 10^{-15}$ ergs s^{-1} cm^{-2} and $C_2(\Delta v = 1)$ flux $F = (3.0 \pm 0.6) \times 10^{-15}$ ergs s^{-1} cm^{-2}. The flux ratio

between $C_2(\Delta v = 0)$ and $C_2(\Delta v = 1)$ is about 1.9. This result is consistent with the fluorescence efficiency L/N of $C_2(\Delta v = 0) = 4.5 \times 10^{-23}$ erg s^{-1} and L/N of $C_2(\Delta v = 1) = 2.4 \times 10^{-23}$ erg s^{-1} (de Almeida et al. 1989), which indicates that the $C_2(\Delta v = 0)$ emission should be about 1.9 times stronger than the emission of $C_2(\Delta v = 1)$. We consider this agreement to be additional evidence suggesting that our C_2 detections are real.

We calculated the C_2 production rate via $C_2(\Delta v = 0)$ emission with the fluorescence efficiency of C_2 and the scale lengths of the parent/daughter molecule adopted from A'Hearn et al. (1995). Assuming that the outflow velocity is 0.58 km s^{-1}, we obtain the production rate $Q(C_2) = (5.5 \pm 0.4) \times 10^{23}$ s^{-1}. This result is below the upper limit estimated by Opitom et al. (2019), and also below or consistent with the measurements of Kareta et al. (2019). The only discrepancy is the LBT observation on 2019 October 10, which is substantially below our estimated value. However, 2I/Borisov was closer to the Sun by 0.245 au during this new measurement (compared to 2019 October 10), so that the C_2 production rate could have increased enough to be detectable.

3.5. Searching for Additional Spectral Features

Besides the main carbon species, we also searched other spectral features such as [O I] at 6300 Å and NH2 emissions across 5500–7500 Å. The spectral beyond 5200 Å is mostly flat, except a weak signal at 6300 Å in the spectrum taken on 2019 October 31 UT (see Figure 2). This signal should belong to [O I] emission. However, since our spectral resolution is low at 6300 Å ($\lambda/\Delta\lambda \sim 120$), we cannot distinguish the cometary [O I] feature from telluric [O I] emission. Therefore, this [O I] feature very likely does not fully belong to the comet.

4. Discussion

In this section we estimate the C_2 production rate as a function of the heliocentric distance (r_h). Kareta et al. (2019) obtained an upper limit of $Q(C_2) < 1.62 \times 10^{23}$ s^{-1}, when the comet was at distance $r_h = 2.39$ au. This study finds $Q(C_2) = (5.5 \pm 0.1) \times 10^{23}$ s^{-1} when the distance has decreased to $r_h = 2.145$ au. As a result, the rate $Q(C_2)$ increased by an increment of at least 3×10^{23} s^{-1} as the body traveled a distance of 0.245 au closer to the Sun. We can calculate the power-law slope γ for the C_2 production rate as a function of r_h, which is given by

$$\gamma = \frac{\log Q(r_{h_1}) - \log Q(r_{h_0})}{\log r_{h_1} - \log r_{h_0}}. \tag{1}$$

With our lower bound of $Q(C_2) \approx 5.1 \times 10^{23}$ s^{-1}, and the upper limit adopted from Kareta et al. (2019), we find a bound on the slope $\gamma < -10.6$. This slope is significantly steeper than those of other comets in our solar system, such as $\gamma = -3.56 \pm 0.16$ for C/2013 R1 (Lovejoy) (Opitom et al. 2015), $\gamma = -4.10 \pm 0.10$ for 103P/Hartley 2 (Knight & Schleicher 2013), and $\gamma = -2.60$ to -4.39 for 81P/Wild 2 (Lin et al. 2012).

The steeper slope for 2I/Borisov suggests that its C_2 production rate might be more sensitive to the heliocentric distance r_h than the solar system comets. On the other hand, if we assume that 2I/Borisov has a $Q(C_2)$ slope that is similar to solar system comets (i.e., $\gamma = -4$), then the rate $Q(C_2)$ would be about 3.5×10^{23} s^{-1} in the middle of 2019 October. This

rate is thus below the MMT upper limit measurement of $Q < 4.4 \times 10^{23}$ s^{-1} (found on 2019 October 9) but higher than the LBT upper limit. With the limited measurements taken to date, it is not possible to draw a firm conclusion on the slope of C_2 production. Follow-up observations and measurements of the C_2 production rate will be needed to solidify these results.

In contrast to the case of C_2, the production rate of CN has not changed dramatically with decreasing distance r_h (see Section 3.2). We adopted all of the $Q(CN)$ measurements from Kareta et al. (2019) and Opitom et al. (2019), and find a power-law slope $\gamma = -2 \pm 1$ for $Q(CN)$ as a function of r_h. This result for the slope of the production rate $Q(CN)$ is similar to that of other solar system comets, where $\gamma = -2.60 \pm 0.17$ for C/2013 R1 (Lovejoy) (Opitom et al. 2015), $\gamma = -3.34 \pm 0.18$ for 103P/Hartley 2 (Knight & Schleicher 2013), and $\gamma = -3.68$ to -2.58 for 81P/Wild 2 (Lin et al. 2012).

Since the observations detected both CN and C_2 emission, we determine the ratio of rates $Q(C_2)/Q(CN) = 0.2 \pm 0.1$. In comparing this value with the observations taken previously, we find that it is below the estimated upper limit of <0.3 by Opitom et al. (2019), but higher than the upper limit of <0.095 from Kareta et al. (2019). Nevertheless, our result of $Q(C_2)/Q(CN) \sim 0.2$ is still consistent with the classification of 2I/Borisov as a carbon-chain-depleted comet. This type of object is more commonly found among the group of JFCs, in contrast to the long-period comets (A'Hearn et al. 1995; Cochran et al. 2012).

We also note that since the C_2 has been detected, the abundances of carbon-chain species are low but not zero. Moreover, all of the current observations of 2I/Borisov, including the reflectance spectrum of its dust coma, the detections of CN and C_2 emission, and the $Q(C_2)/Q(CN)$ ratio, indicate that its properties are similar to ordinary comets found in our solar system. This finding, in turn, suggests that the natal disk of 2I/Borisov formed could have a similar chemical composition to our solar system.

5. Summary

In this study, we report the spectroscopic observations of 2I/Borisov on 2019 October 31.5 and November 4.5 UT using the Hiltner 2.4 m telescopes and the OSMOS Spectrograph on the MDM Observatory. We find that the dust coma reflectance is a function of wavelength, which is steeper for shorter wavelengths ($9.2\%/10^3$ Å) and shallower at longer wavelengths ($19.3\%/10^3$ Å). Emission from both CN and C_2 were detected, with possible but unconfirmed C_3 emission. We estimated the CN production rate $Q(CN) = (2.0 \pm 0.2) \times 10^{24}$ s^{-1} on 2019 November 1 and $Q(CN) = (2.4 \pm 0.2) \times 10^{24}$ s^{-1} on 2019 November 5. The C_2 production rate was also estimated by coadding the spectra on 2019 October 31 and November 4, with the value of $Q(C_2) = (5.5 \pm 0.4) \times 10^{23}$ s^{-1}. Comparing our production rates with the upper limit obtained by Kareta et al. (2019), we find that the rate $Q(C_2)$ of 2I/Borisov might be relatively more sensitive to heliocentric distance than other solar system comets. We computed the ratio $Q(C_2)/Q(CN) = 0.2 \pm 0.1$, which indicates that 2I/Borisov is a carbon-chain-depleted comet. Given that most of the properties currently known about 2I/Borisov are similar to known solar system comets, this interstellar visitor is likely to have formed within a planetary system much like our own.

ORCID iDs

Hsing Wen Lin
(林省文) ● https://orcid.org/0000-0001-7737-6784
Chien-Hsiu Lee
(李見修) ● https://orcid.org/0000-0003-1700-5740
D. W. Gerdes ● https://orcid.org/0000-0001-6942-2736
Fred C. Adams ● https://orcid.org/0000-0002-8167-1767
Juliette Becker ● https://orcid.org/0000-0002-7733-4522
Kevin Napier ● https://orcid.org/0000-0003-4827-5049

References

A'Hearn, M. F., Millis, R. C., Schleicher, D. O., Osip, D. J., & Birch, P. V. 1995, Icar, 118, 223

Astropy Collaboration, Price-Whelan, A. M., Sipőcz, B. M., et al. 2018, AJ, 156, 123

Astropy Collaboration, Robitaille, T. P., Tollerud, E. J., et al. 2013, A&A, 558, A33

Bolin, B. T., Lisse, C. M., Kasliwal, M. M., et al. 2019, arXiv:1910.14004

Cochran, A. L., Barker, E. S., & Gray, C. L. 2012, Icar, 218, 144

Cochran, A. L., & Schleicher, D. G. 1993, Icar, 105, 235

de Almeida, A. A., Singh, P. D., & Burgoyne, C. M. 1989, EM&P, 47, 15

de León, J., Licandro, J., Serra-Ricart, M., et al. 2019, RNAAS, 3, 131

Feibelman, W. A., Hyung, S., & Aller, L. H. 1996, MNRAS, 278, 625

Fitzsimmons, A., Hainaut, O., Meech, K. J., et al. 2019, ApJL, 885, L9

Guzik, P., Drahus, M., Rusek, K., et al. 2019, NatAs, 4, 53

Haser, L. 1957, BSRSL, 43, 740

Hunter, J. D. 2007, CSE, 9, 90

Jewitt, D., Hui, M.-T., Kim, Y., et al. 2020, ApJL, 888, L23

Jewitt, D., & Luu, J. 2019, ApJL, 886, L29

Jewitt, D., & Meech, K. J. 1986, ApJ, 310, 937

Kareta, T., Andrews, J., Noonan, J. W., et al. 2019, arXiv:1910.03222

Knight, M. M., & Schleicher, D. G. 2013, Icar, 222, 691

Lee, C.-H., Lin, H.-W., Chen, Y.-T., & Yen, S.-F. 2019, RNAAS, 3, 184

Lin, Z. Y., Lara, L. M., Vincent, J. B., & Ip, W. H. 2012, A&A, 537, A101

Martini, P., Stoll, R., Derwent, M. A., et al. 2011, PASP, 123, 187

McKay, A. J., Cochran, A. L., Dello Russo, N., & DiSanti, M. 2019, arXiv:1910.12785

Meech, K. J., Weryk, R., Micheli, M., et al. 2017, Natur, 552, 378

Mommert, M., Kelley, M., de Val-Borro, M., et al. 2019, JOSS, 4, 1426

Opitom, C., Fitzsimmons, A., Jehin, E., et al. 2019, A&A, 631, L8

Opitom, C., Jehin, E., Manfroid, J., et al. 2015, A&A, 584, A121

Schleicher, D. G. 2010, AJ, 140, 973

Virtanen, P., Gommers, R., Oliphant, T. E., et al. 2019, arXiv:1907.10121

Yang, B., Kelley, M. S. P., Meech, K. J., et al. 2020, A&A, in press

Ye, Q., Kelley, M. S. P., Bolin, B. T., et al. 2019, arXiv:1911.05902